Supplementary Information for

General strategy for activating ferroelectricity in bilayer 2D materials with intercalating inert atoms

Wenqi Xiong[1,*] and Yu Jia[1,2]

[1]*Institute of Quantum Materials and Physics, Henan Academy of Sciences, Zhengzhou 450046, China*

[2]*Key Laboratory for Special Functional Materials of the Ministry of Education, School of Nanoscience and Materials Engineering, Henan University, Zhengzhou 450046, China*

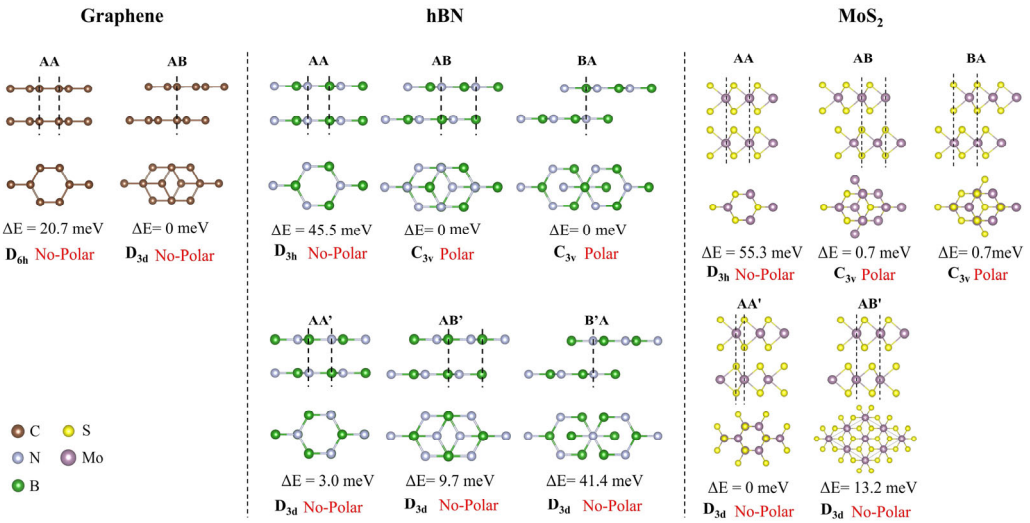

Fig. S1. Side and top views of atomic structures for bilayer graphene, hBN, and MoS_2 in different stacking configurations, along with their relative energies (ΔE), point group symmetries, and polarities.

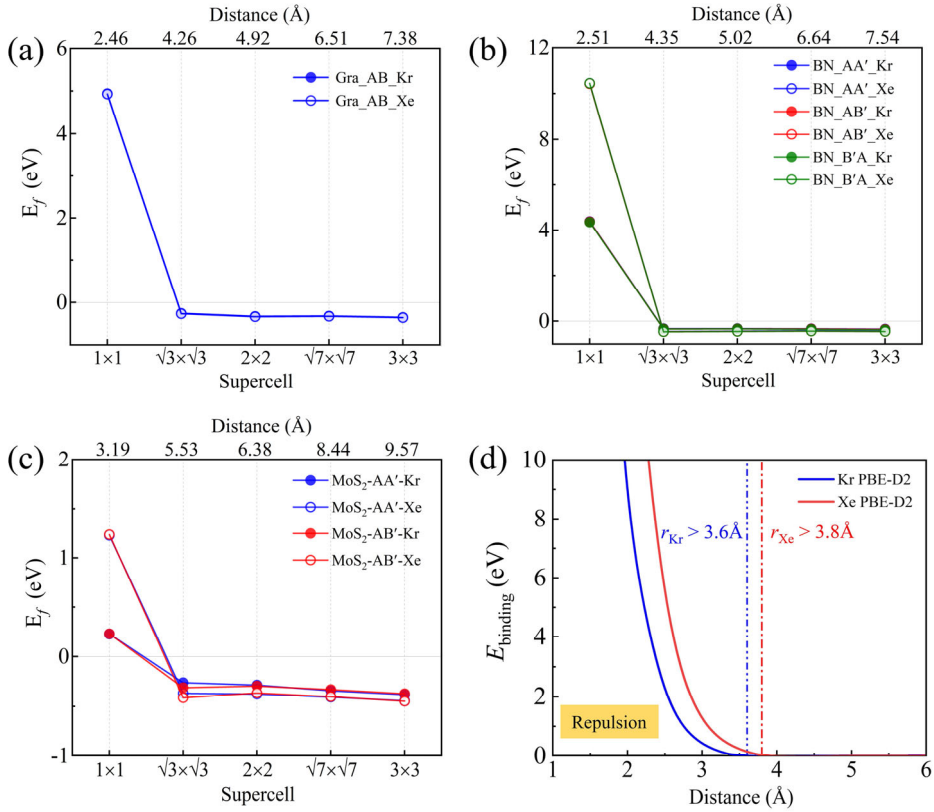

Fig. S2. Formation energy (E_f) of inert atoms intercalated in bilayer (**a**) graphene, (**b**) h-BN, and (**c**) MoS_2 as a function of supercell size and inert-atom distance. **d** Binding energy ($E_{binding}$) between two inert atoms as a function of supercell size and inert-atom distance. The vertical dashed line marks the critical distances where $E_{binding} = 0$. The binding energy approaches zero at large separations (> 4Å), indicating negligible interaction, while its increase at shorter distances reflects the emergence of strong repulsion.

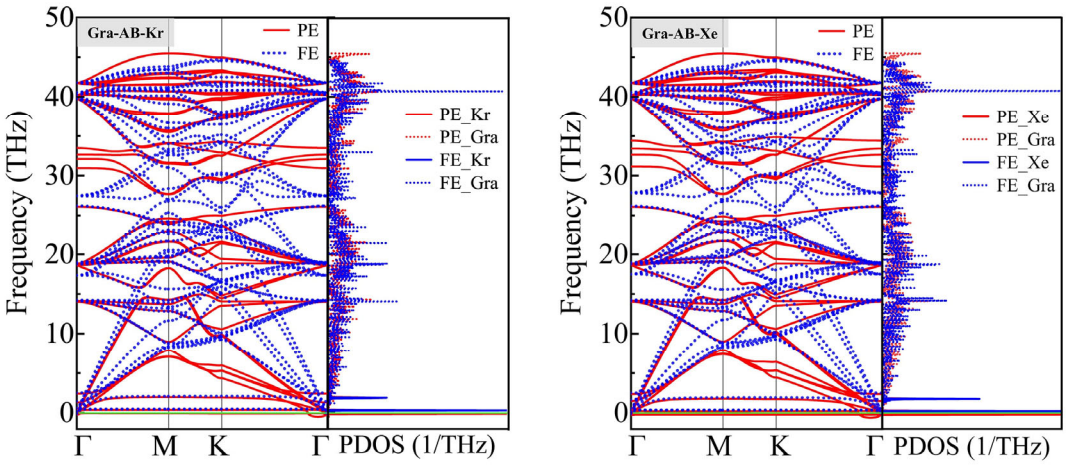

Fig. S3. Phonon spectra and projected DOS of FE and PE phases for Kr/Xe-intercalated graphene bilayers. The green horizontal line represents the phonon mode with zero energy.

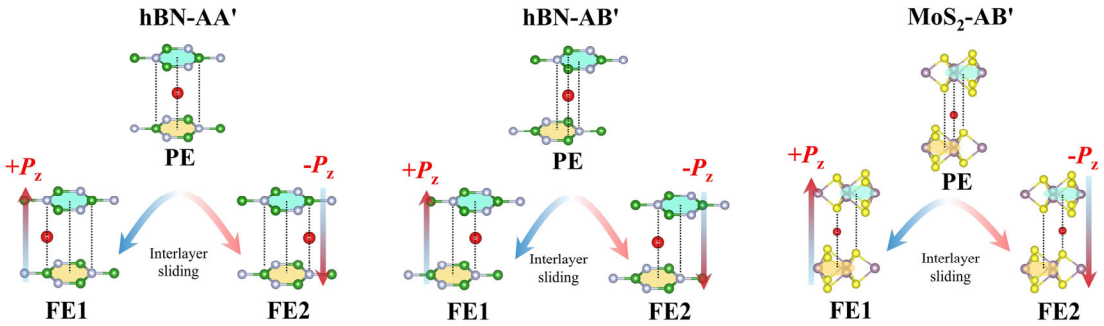

Fig. S4. Side views of the FE and PE states of inert-atom-intercalated AA′- and AB′-stacked bilayer hBN, AB′-stacked bilayer MoS_2. The red balls represent inert atoms Kr/Xe.

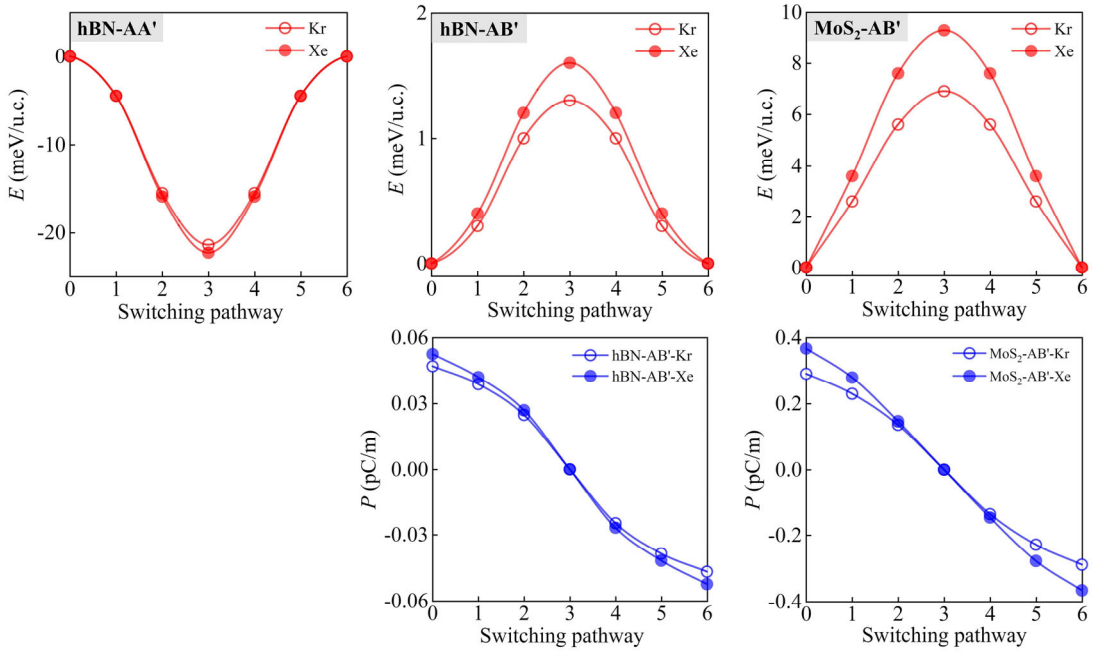

Fig. S5. Energy barriers and OOP electric polarization of inert-atom-intercalated AA′- and AB′-stacked bilayer hBN, AB′-stacked bilayer MoS_2. Due to the instability of the FE state in Xe-intercalated AA′-stacked hBN, the polarization associated with FE switching is absent.

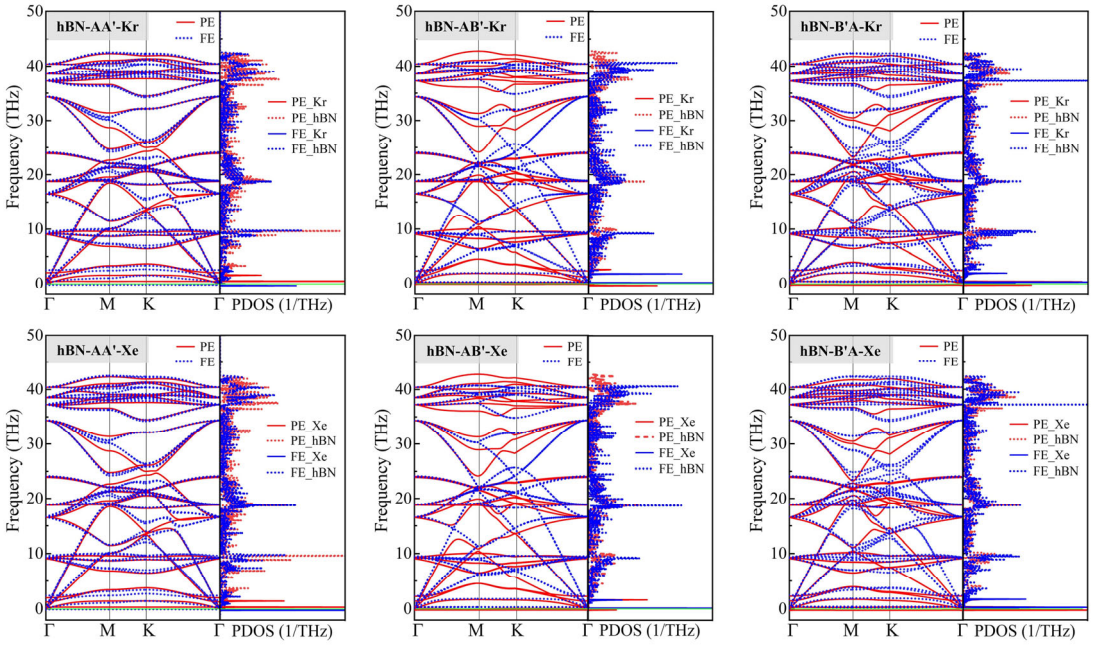

Fig. S6. Phonon spectra and projected DOS of FE and PE phases for Kr/Xe-intercalated hBN bilayers. The green horizontal line represents the phonon mode with zero energy.

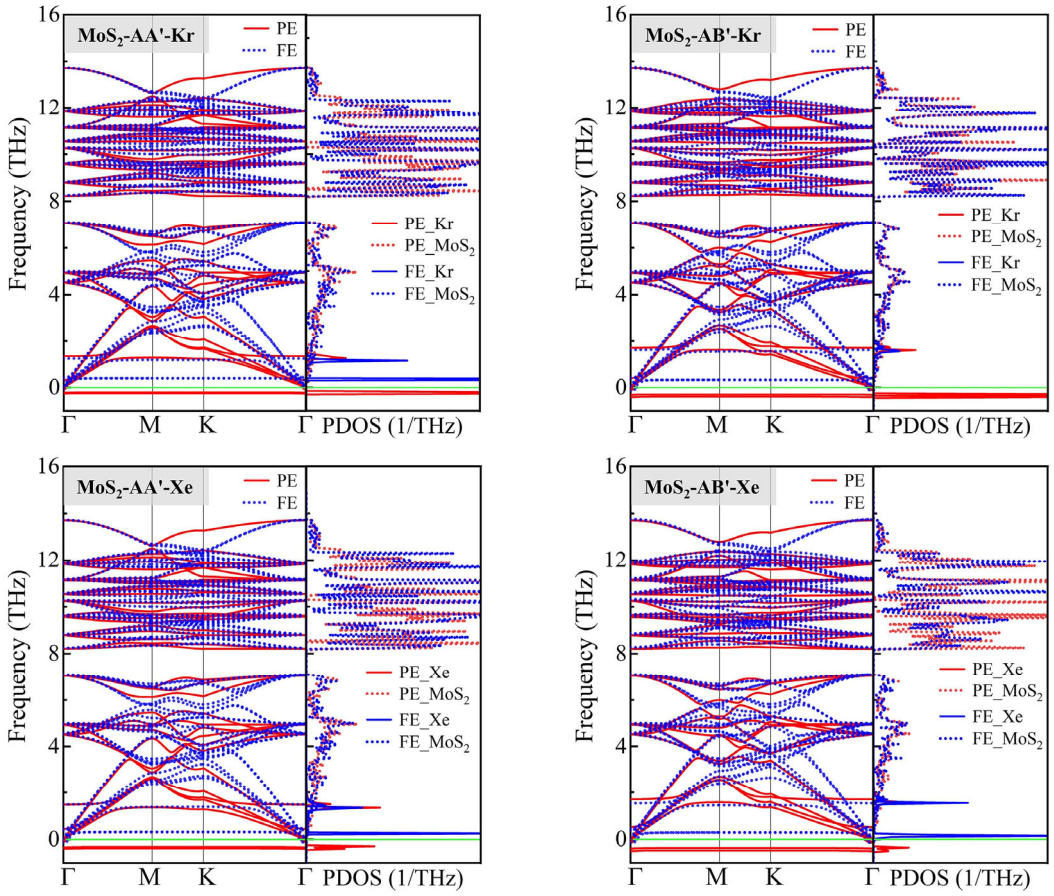

Fig. S7. Phonon spectra and projected DOS of FE and PE phases for Kr/Xe-intercalated MoS_2 bilayers. The green horizontal line represents the phonon mode with zero energy.

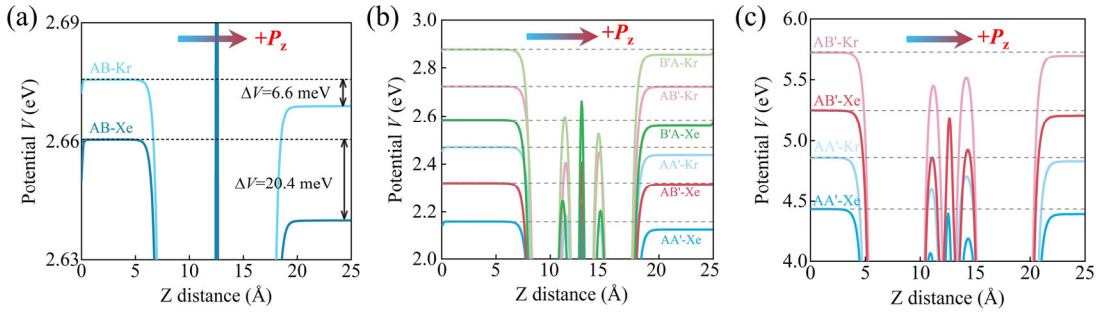

Fig. S8. Planar-averaged electrostatic potential of the FE states for inert-atom-intercalated bilayers.

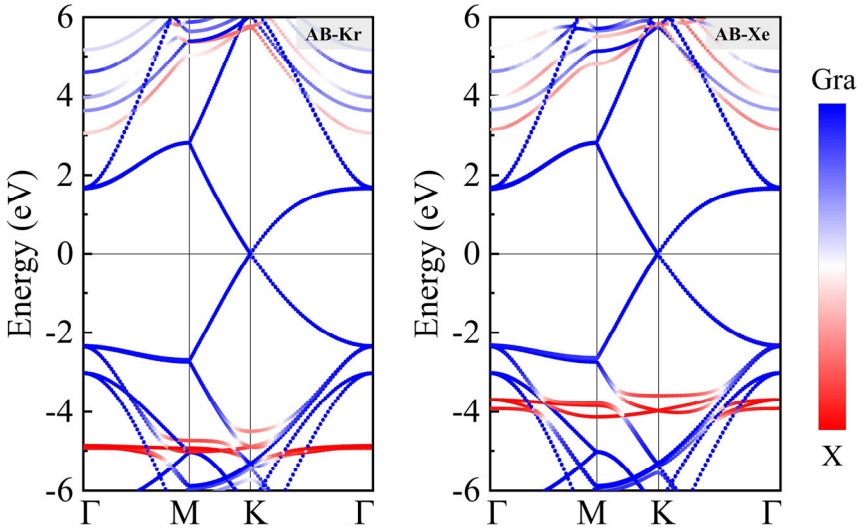

Fig. S9. Atomically resolved band structures for inert-atom-intercalated bilayer graphene.

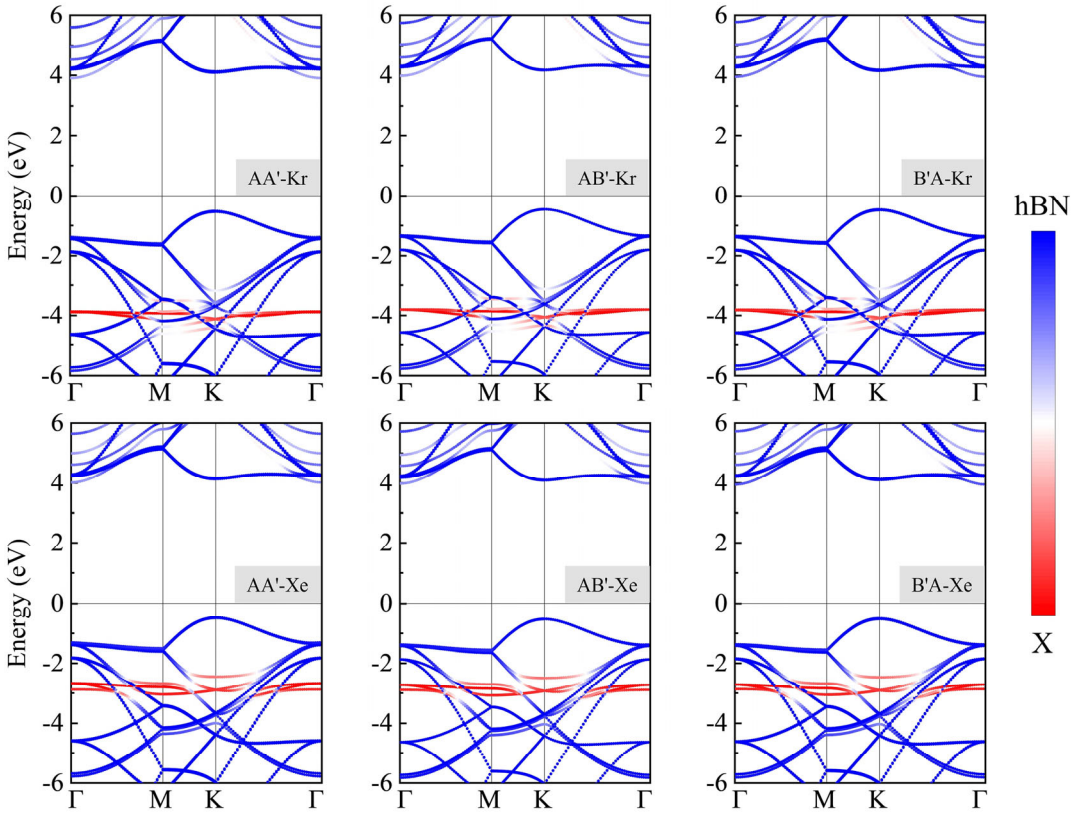

Fig. S10. Atomically resolved band structures for inert-atom-intercalated bilayer hBN.

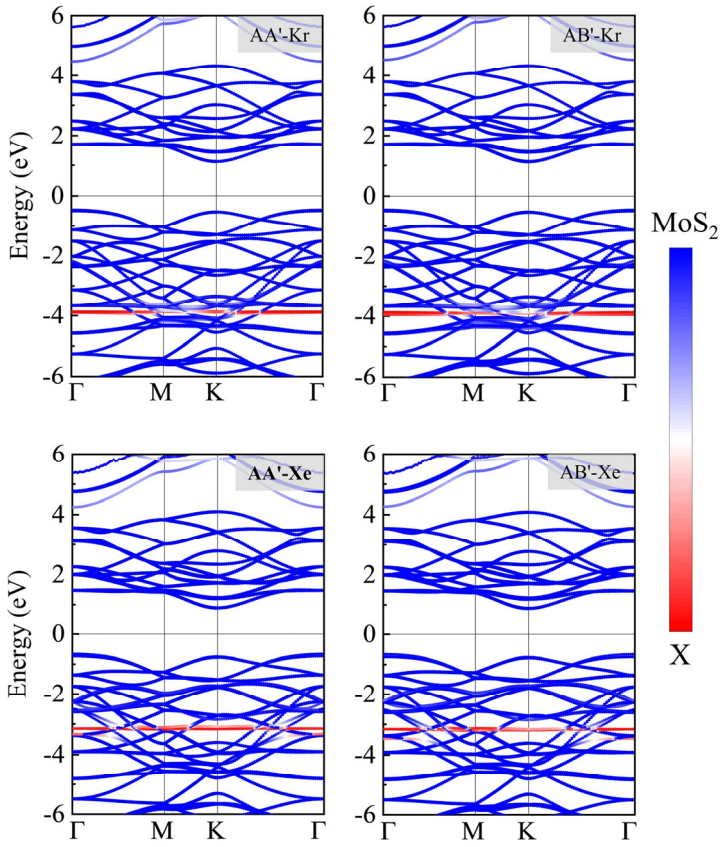

Fig. S11. Atomically resolved band structures for inert-atom-intercalated bilayer MoS_2.

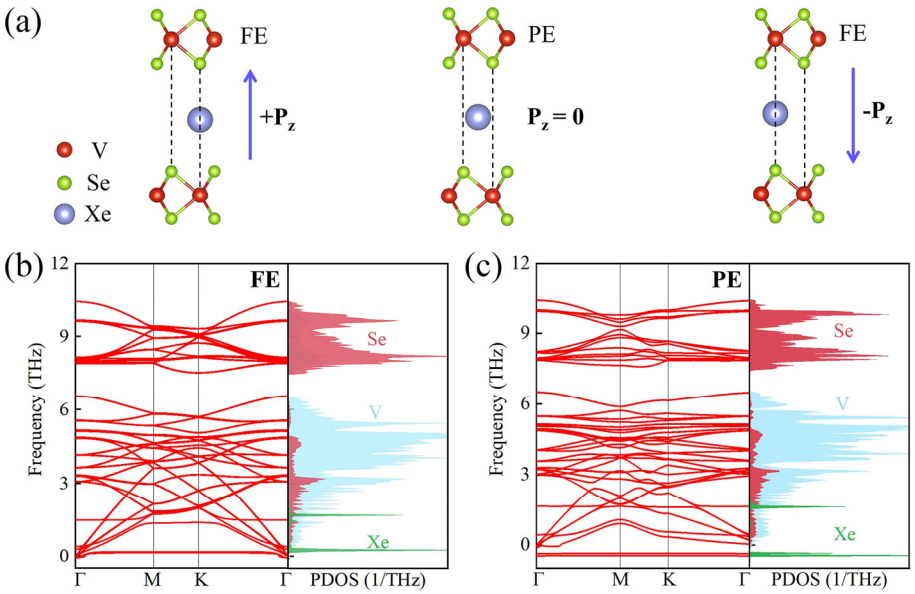

Fig. S12. (**a**) Side views of the FE and PE states of Xe-intercalated AA′-stacked 2×2×1 bilayer VSe_2. The FE polarization P_z is 0.25 pC/m. Phonon spectra and projected DOS of (**b**) FE and (**c**) PE states. No imaginary phonon modes are observed in the FE phase, whereas the PE phase exhibits clear imaginary branches.

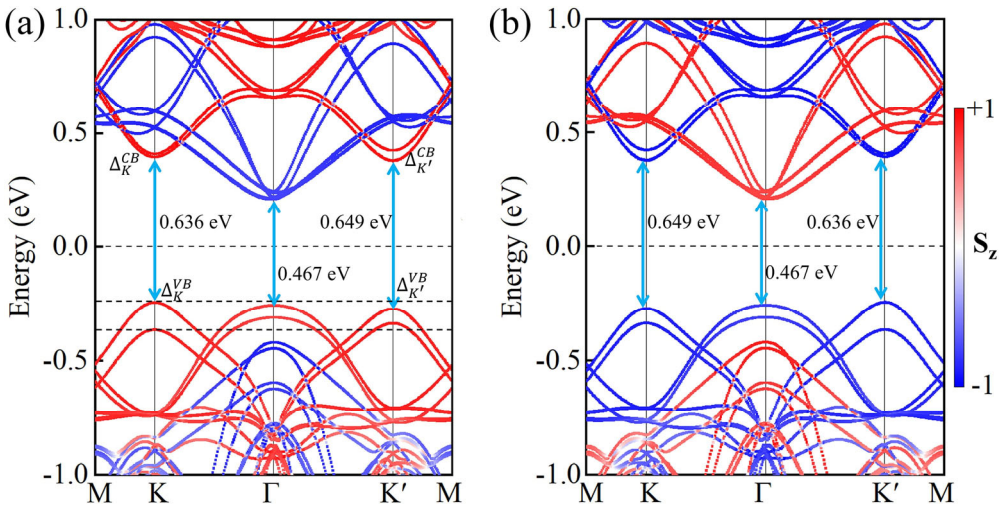

Fig. S13. Spin-resolved band structures of Xe-intercalated bilayer VSe_2 with spin-orbit coupling under (**a**) $+P_z$ and (**b**) $-P_z$ states. The color bar represents the spin contribution of the energy band, in which +1 and -1 represent two opposite spin directions (S_z), respectively. The PBE+U (U = 1.0 eV) method was adopted. The Fermi level is set to 0 eV. $\Delta_K^{CB} = 13\ meV$, $\Delta_{K'}^{CB} = 45\ meV$, $\Delta_K^{VB} = 122\ meV$, and $\Delta_{K'}^{VB} = 65\ meV$.

Linear relationship between OOP polarization and electrostatic potential difference

To elucidate the origin of out-of-plane ferroelectricity induced by intercalated inert atoms in bilayers, we establish the relation between the spontaneous polarization P and the electrostatic potential difference ΔV. Upon intercalation of noble gas atoms (e.g., Kr, Xe) into the van der Waals gap, the system symmetry is reduced from centrosymmetric D_{3d} to polar C_{3v}, leading to asymmetric charge redistribution and net electric polarization.

In a simplified dipole model, this asymmetric charge distribution can be treated as an electric dipole formed by partial charge displacement $\pm q$ across an effective separation distance d, corresponding to the vertical shift between the top and bottom layers or charge centers. The total dipole moment per unit cell is given by $p = q \cdot d$, and the spontaneous polarization is defined as:

$$P = p/A = (q \cdot d)/A\,, \tag{S1}$$

where A is the in-plane area of the unit cell. The induced polarization generates an internal electric field $E = P/(\varepsilon_0 \varepsilon_r)$, which in turn gives rise to an electrostatic potential difference:

$$\Delta V = E \cdot d = \frac{P \cdot d}{\varepsilon_0 \varepsilon_r} \Longrightarrow P = \frac{\varepsilon_0 \varepsilon_r}{d} \cdot \Delta V, \tag{S2}$$

where ε_0 and ε_r are the vacuum dielectric constant and effective dielectric constant, respectively. The proportionality factor $\alpha = \varepsilon_0 \varepsilon_r / d$ depends on the interlayer distance d and the effective dielectric constant ε_r. Table S1 lists the interlayer spacing d and dielectric constants ε_r of graphene, hBN, and MoS_2. Substituting these parameters into the proportionality factor reveals that the systems remain within the linear polarization response regime. Although the precise values of ε_r and d may vary slightly between different materials, the linear trend persists due to the self-consistent nature of the polarization and electrostatic potential.

Table S1. Interlayer spacing and dielectric constants of graphene, hBN, and MoS_2 reported in literatures.

Materials	Distance d (Å)	Effective dielectric constant ε_r	Ref.
Graphene	3.4	3	[1,2]
hBN	3.5 ~ 3.8	3.3	[3,4]
MoS_2	3.1 ~ 3.7	3.4	[5,6]

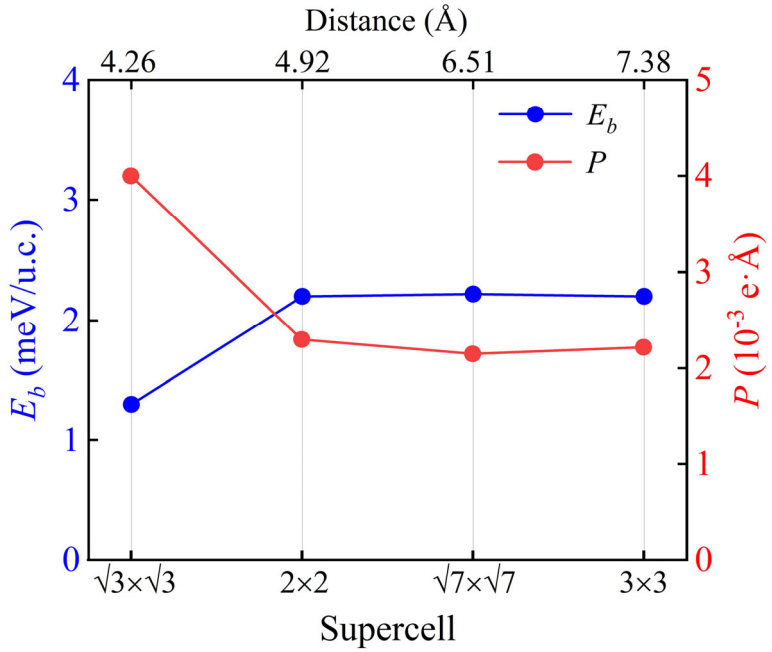

Fig. S14. Switching barriers (E_b) and FE polarizations (P) of Xe-intercalated AB-stacked bilayer graphene as a function of supercell size and inert-atom distance.

References:

[1] V. Despoja, Z. Rukelj, and L. Marušić, *Ab initio* study of electronic excitations and the dielectric function in molybdenum disulfide monolayer, Phys. Rev. B **94**, 165446 (2016).

[2] I. Brihuega, P. Mallet, H. González-Herrero, G. Trambly De Laissardière, M. M. Ugeda, L. Magaud, J. M. Gómez-Rodríguez, F. Ynduráin, and J.-Y. Veuillen, Unraveling the Intrinsic and Robust Nature of van Hove Singularities in Twisted Bilayer Graphene by Scanning Tunneling Microscopy and Theoretical Analysis, Phys. Rev. Lett. **109**, 196802 (2012).

[3] A. Laturia, M. L. Van de Put, and W. G. Vandenberghe, Dielectric properties of hexagonal boron nitride and transition metal dichalcogenides: from monolayer to bulk, Npj 2D Mater. Appl. **2**, 6 (2018).

[4] R. M. Ribeiro and N. M. R. Peres, Stability of boron nitride bilayers: Ground-state energies, interlayer distances, and tight-binding description, Phys. Rev. B **83**, 235312 (2011).

[5] E. J. G. Santos and E. Kaxiras, Electric-Field Dependence of the Effective Dielectric Constant in Graphene, Nano Lett. **13**, 898 (2013).

[6] J. T. Jiang, S. L. Xiu, M. M. Zheng, T. T. Jia, H. Y. Liu, Y. Zhang, and G. Chen, Indirect–direct bandgap transition and gap width tuning in bilayer MoS2 superlattices, Chem. Phys. Lett. **613**, 74 (2014).